Separation and Purification Technology 130 (2014) 19–27

Contents lists available at ScienceDirect

Separation and Purification Technology

journal homepage: www.elsevier.com/locate/seppur

Coagulation and sludge recovery using titanium tetrachloride as coagulant for real water treatment: A comparison against traditional aluminum and iron salts

Y.X. Zhao [a], B.Y. Gao [a,*], G.Z. Zhang [a], Q.B. Qi [a], Y. Wang [a], S. Phuntsho [b], J.-H. Kim [c], H.K. Shon [b], Q.Y. Yue [a], Q. Li [a]

[a] Shandong Key Laboratory of Water Pollution Control and Resource Reuse, School of Environmental Science and Engineering, Shandong University, No. 27 Shanda South Road, Jinan 250100, People's Republic of China
[b] Centre for Technology in Water and Wastewater, School of Civil and Environmental Engineering, University of Technology, Sydney (UTS), P.O. Box 123, Broadway, NSW 2007, Australia
[c] School of Applied Chemical Engineering, The Institute for Catalysis Research, Chonnam National University, Gwangju 500-757, South Korea

ARTICLE INFO

Article history:
Received 13 June 2013
Received in revised form 29 March 2014
Accepted 6 April 2014
Available online 18 April 2014

Keywords:
Coagulation–flocculation
Titanium tetrachloride
Floc strength
Floc recovery
Sludge recovery

ABSTRACT

Coagulation/flocculation performance of titanium tetrachloride ($TiCl_4$), ferric chloride ($FeCl_3$) and aluminum sulfate ($Al_2(SO_4)_3$) was comparatively investigated for real water treatment. Comparisons were made under different coagulant dose and initial solution pH conditions and their performances measured in terms of UV_{254} (absorbance at 254 nm) and DOC (dissolved organic carbon) removal and residual turbidity. Characteristics of aggregated flocs during the coagulation/flocculation process by the three coagulants were studied using a laser diffraction particle sizing device. The performances of the three coagulants were also assessed in terms of the membrane fouling potential of the ultrafiltration (UF) membrane or during coagulation–ultrafiltration (C–UF) process using a stirred and dead-end batch UF unit. Additionally, the $TiCl_4$ flocculated sludge was recovered to produce titanium dioxide (TiO_2) under thermal treatment. The results indicate that the $TiCl_4$ showed superior coagulation performance compared to that of $FeCl_3$ and $Al_2(SO_4)_3$, with the optimum removal of UV_{254} and DOC of 54.9% and 55.1%, respectively. The aggregated flocs formed by $TiCl_4$ showed the highest growth rate with the largest size compared to those by $FeCl_3$ and $Al_2(SO_4)_3$, but with the weakest floc strength and the worst re-growth ability. The $TiCl_4$ and $FeCl_3$ yielded the flocs with comparable degree of compaction, higher than that by $Al_2(SO_4)_3$. Additionally, the investigation of membrane fouling demonstrated that the severity of flux decline followed the order of $Al_2(SO_4)_3 < FeCl_3 < TiCl_4$. $TiCl_4$ coagulated sludge was also characterized by X-ray diffraction, Thermal analysis and scanning electron microscope.

1. Introduction

Coagulation–flocculation is one of the most common and important water treatment processes for particle and natural organic matter (NOM) removal [1]. Using conventional Al and Fe salts as coagulants suffers from two major issues or challenges: toxicity of the residual coagulant and sludge production [2,3]. The significant advantage of using titanium tetrachloride ($TiCl_4$) as a coagulant is that, its flocculated sludge can be recovered to produce a valuable by-product, namely titanium dioxide (TiO_2) by thermal treatment, which is not possible with the conventional coagulants [3,4]. TiO_2 is the most widely used metal oxide, whose applications include photocatalysts, cosmetics, paints, electronic paper, and solar cells [5,6]. The toxicity of the supernatant after $TiCl_4$ coagulation is very low, and the residual Ti salt concentration in the treated water meets the World Health Organization's (WHO) guidelines (0.5–15 μg/L) for drinking water standards [7]. Therefore, $TiCl_4$ is expected to be a promising alternative coagulant to the conventional Al and Fe salts.

The size and strength of flocs formed during the coagulation/flocculation process are considered fundamental to the separation and purification process [8]. Regions of high shear force, such as areas around the impeller zone of flocculating tanks and transfer over weirs and ledges, are prevalent in units at water treatment works [9]. The resultant broken flocs with reduced sizes result in lower sedimentation rate and may not only contaminate the filter (depending on the pore size and filter thickness), which may result

* Corresponding author. Tel.: +86 531 88366771; fax: +86 531 88364513.
E-mail address: baoyugao_sdu@aliyun.co (B.Y. Gao).

http://dx.doi.org/10.1016/j.seppur.2014.04.015
1383-5866/

in lower filtration performance, but also may pass through the filter resulting in the incomplete separation [10]. In addition, newly exposed surface of the aggregates may alter the surface charge of the floc aggregates, leading to partial re-stabilization [9]. Moreover, the floc shapes (often described in terms of fractal geometry concept or the fractal dimension) affected particle behavior, particularly with regard to collision efficiency and settling rates [11,12]. Therefore, floc size, strength, recoverability and structure are considered as important parameters to provide valuable information in understanding coagulation performance and coagulation mechanisms of a new coagulant, while few researches have focused on those by $TiCl_4$. Since $TiCl_4$ is only studied recently as a novel coagulant, only few of these parameters are accurately assessed and compared with the conventional coagulants.

Recently, ultrafiltration (UF) technology has been widely used for removal of suspended solids, colloidal material, NOM and disinfection byproducts precursors [13,14]. Due to serious membrane fouling and poor NOM removal, coagulation pretreatment prior to membrane filtration has been suggested both for improving NOM removal and for reducing membrane fouling [15–17]. The practical effects of precoagulation using conventional Al and Fe salts on membrane fouling have been widely investigated [18–20]. The coagulant type and floc characteristics are believed to play significant roles in membrane fouling [21–23]. However, none of the previous studies have addressed the effect of $TiCl_4$ precoagulation on the performance of membrane process particularly in the fouling potential of UF membrane in the coagulation–ultrafiltration (C–UF) hybrid process.

Therefore the main objectives of this study are to (i) evaluate the coagulation performance of $TiCl_4$ in real water treatment and compare to traditional $Al_2(SO_4)_3$ and $FeCl_3$ coagulants, (ii) characterize the floc properties using a laser diffraction instrument, and (iii) investigate the mechanisms involved in the coagulation–flocculation process based on coagulation performance, floc properties and zeta potential measurement, (iv) comparatively investigate the membrane performance with different coagulants in C–UF hybrid process, and (v) produce TiO_2 from the $TiCl_4$ flocculated sludge and study its characteristics by X-ray diffraction (XRD) analysis, Thermal analysis and scanning electron microscope (SEM).

2. Experimental

2.1. Coagulants and test water

$TiCl_4$ solution (20%, density = 1.150 g/mL) was obtained from Photo & Environment Technology Co. Ltd. (South Korea), and was used directly without any pretreatment. Stock solutions of $Al_2(SO_4)_3$ and $FeCl_3$ were prepared at a concentration of 1 g/L by Al and 2 g/L by Fe, respectively. Deionized water was used for all the reagent preparation.

The water source used in this study was withdrawn from Xiaoqing River, which is the main drainage channel in central region of Shandong Province, China and also plays an important role for farmland irrigation. The water was collected in spring season, and the water temperature was at 10–15 °C. The turbidity, UV_{254} absorbance, DOC, zeta potential and pH of the simulated water were 6.20–9.44 NTU, 0.067–0.073 cm^{-1}, 3.90–4.55 mg/L, −11.0 ± 1.0 mV and 7.95–8.46, respectively.

2.2. Jar-test

Standard jar tests were conducted using a programmable jar-tester. Detailed experimental procedures are described in S1 of the Supplementary data (SD).

Coagulation–flocculation experiments under different solution pH values were conducted after the optimal coagulant dosages were determined. The target coagulation pH values were achieved by adding appropriate quantities of HCl and NaOH solutions with the concentration of 0.1 mol/L.

2.3. Determination of dynamic floc properties

A laser diffraction instrument (Mastersizer 2000, Malvern, UK) was used to measure dynamic floc size as the coagulation and flocculation process proceeded. The schematic diagram of the on-line monitoring system for dynamic floc size can be found in Zhao et al. [24].

Following the floc growth phase, the aggregated flocs were exposed to a shear force at 200 rpm for 1 min, followed by a slow mixing at 40 rpm for 15 min to allow floc regrowth. The median equivalent diameter, d_{50}, was selected as the representative floc size, although the same trends were observed for d_{10} and d_{90} floc sizes.

The floc growth rate was calculated by the slope of the rapid growth region [25]:

$$\text{Growth rate} = \frac{\Delta size}{\Delta time} \tag{1}$$

Floc strength factor (S_f) and recovery factor (R_f) are used to compare the floc breakage and recoverability [24,26–28]:

$$S_f = \frac{d_2}{d_1} \times 100 \tag{2}$$

$$R_f = \frac{d_3 - d_2}{d_1 - d_2} \times 100 \tag{3}$$

where d_1 is the average floc size of the plateau before breakage, d_2 is the floc size after the floc breakage period, and d_3 is the floc size after regrowth to the new plateau.

Previous researches have reported the determination of aggregate mass fractal dimension (D_f) by using Mastersizer 2000 [27,29,30]. The total scattered light intensity I, the scattering vector Q, and D_f followed a power law [31]:

$$I \propto Q^{-Df} \tag{4}$$

The scattering vector Q is the difference between the incident and scattered wave vectors of the radiation beam in the medium [29]:

$$Q = \frac{4n\pi \sin(\theta/2)}{\lambda} \tag{5}$$

where n, λ and θ are the refractive index of the medium, the laser light wavelength in vacuum, and the scattering angle, respectively.

Densely packed aggregate has a higher D_f value, while lower D_f value results from a large, high branched and loose bound structure.

2.4. Coagulation–ultrafiltration (C–UF)

UF membrane with a molecular weight cut-off (MWCO) of 100 kDa was provided by Mosu Shanghai. All the UF experiments were carried out using a magnetically stirred cell (MSC050, Mosu, China), with a total holding capacity of 300 mL and an effective membrane area of 50.2 cm^2. The cell was pressurized with nitrogen gas at 0.15 ± 0.05 MPa without shaking. An electronic balance (MSU5201S-000-D0, SARTORIUS AG GERMANY) connected to PC was employed to measure mass of the UF permeate. The mass data was recorded every 10 s and the flux decline with time was calculated to assess the membrane fouling. Schematic diagrams of the experiment of C–UF hybrid process can be found in the reference [18].

2.5. TiO_2 preparation and characterization from the flocculated sludge

Sludge produced from $TiCl_4$ coagulation was freeze-dried with ultra-low temperature refrigerated storage box DW-HL100 and freezer dryer FD-1A-50, followed by calcination in a furnace at 200 °C, 400 °C, 600 °C, 800 °C and 1000 °C for 12 h duration [3].

XRD analysis was performed with Rigaku (Japan) D/MAX-rA diffractometer (Cu Kα radiation) while the microstructures were characterized using JSM-7600F SEM (Japanese electronics Co., Ltd. (JEOL)).

Thermal behavior was tested to determine sintering temperature by thermogravimetry (TG) and differential scanning calorimetry (DSC), using a Q600 SDT synchronization heat analyzer. The $TiCl_4$ flocculated sludge was heated from room temperature (22 °C) to 1000 °C at a rate of 10 °C/min in air atmosphere.

3. Results and discussion

3.1. Coagulation performance as a function of coagulant dose

The merits of $TiCl_4$ coagulation–flocculation performance was evaluated in terms of particles and organic matter removal and compared with the performances of the commonly used $FeCl_3$ and $Al_2(SO_4)_3$ coagulants. Fig. 1 shows the coagulation efficiencies of the three coagulants as a function of coagulant dose (10–80 mg/L for $TiCl_4$ as Ti, 15–90 mg/L $FeCl_3$ as Fe and 5–50 mg/L $Al_2(SO_4)_3$ for as Al).

For both $TiCl_4$ and $FeCl_3$, the residual turbidity of effluents decreased with the increase in coagulant dose however, beyond certain dosage, the residual turbidity consistently increased with the coagulant dose. On the other hand, a gradual increase of residual turbidity with coagulant dose was observed for $Al_2(SO_4)_3$. The removal trend for UV_{254} and DOC were quite similar for all three coagulants which increased significantly first with the increase of coagulant dose and then approached a plateau or showed slight decrease at high coagulant doses. Considering the coagulation efficiency and cost, the optimum doses for $TiCl_4$, $FeCl_3$ and $Al_2(SO_4)_3$ were fixed at 70 mg/L, 65 mg/L and 30 mg/L, respectively, above which point the NOM removal efficiencies did not vary significantly. Under the optimum dose conditions, $TiCl_4$ was superior to both $FeCl_3$ and $Al_2(SO_4)_3$ in UV_{254} removal with the order of $TiCl_4$ (54.7%) > $FeCl_3$ (46.6%) > $Al_2(SO_4)_3$ (36.8%). The DOC removal by $TiCl_4$ and $FeCl_3$ was around 50% higher than 37% by $Al_2(SO_4)_3$. Additionally, the flocs formed by $TiCl_4$ showed higher sedimentation velocity, which suggests that $TiCl_4$ needs much shorter retention time and offers significant advantage in terms of the size of the sedimentation tanks. More details on this can be found in S2 of the SD.

Fig. 1 also shows the variations of floc zeta potential with coagulant dose for the three coagulants. The zeta potentials increased gradually with coagulant concentration and then reached isoelectric points at the $TiCl_4$ dose of about 70 mg/L, $FeCl_3$ dose of about 60 mg/L and $Al_2(SO_4)_3$ dose of around 15 mg/L. Further increased the coagulant dose led to floc charge reversal. As previously reported, the dosage at which the charge reversal occurs was defined as iso-electrical-dosage (IED) [32]. Thus, the IED values for $TiCl_4$, $FeCl_3$ and $Al_2(SO_4)_3$ were about 70, 60 and 15 mg/L, respectively, indicating the charge neutralization capability order of $Al_2(SO_4)_3$ > $FeCl_3$ > $TiCl_4$. According to Licsko [33], the hydrolysis of metal ions occurred immediately after contacting with water and thus the charge neutralization capability of coagulants was tightly associated with the positive charges of their corresponding hydrolyzed species. The weaker charge neutralization ability of $TiCl_4$ than $FeCl_3$ and $Al_2(SO_4)_3$ implied the corresponding hydrolyzates were with less positive charges to support the efficient charge neutralization. This is quite in contrast to the previous study by Mekhamer and Assaad [34], who reported that the higher the charge of a cation, the stronger is its effect on particle zeta potential and the higher the valance, the higher the coagulative power. Changes in floc zeta potential are not only used to evaluate the destabilization ability of coagulants, but also are generally regarded as effective tool to investigate coagulation mechanism. Coagulation is generally explained in terms of charge neutralization and sweep flocculation [35]. Particle removal using metal coagulants has long been recognized under conditions of rapid and extensive hydroxide precipitation. In this study, bulk precipitation of metal hydroxide occurred under optimum dose conditions, producing the flocs with particle zeta potentials for $TiCl_4$, $FeCl_3$ and $Al_2(SO_4)_3$ of +3.8, +1.4 and +4.5 mV, respectively. This indicated that sweep flocculation played an important role besides charge neutralization.

3.2. Effect of initial solution pH on coagulation performance

At the optimum dose of each coagulant, the variation of residual turbidity, UV_{254} and DOC removal, and the floc zeta potential as a function of initial solution pH shown in Fig. 2. Overall, the turbidity removal was seldom affected by initial solution pH for $Al_2(SO_4)_3$, with the residual turbidity varied from 1.6 to 4.2 NTU within the pH range investigated. Whilst for both $TiCl_4$ and $FeCl_3$, high solution pH favored the turbidity removal, as reflected by the significant lower residual turbidity in neutral and alkaline conditions than that in acidic conditions. The $Al_2(SO_4)_3$ coagulant was superior in turbidity removal to both $TiCl_4$ and $FeCl_3$ in acidic conditions, where the residual turbidity was higher than 30 NTU for both $TiCl_4$ and $FeCl_3$, while that was lower than 4.2 NTU for $Al_2(SO_4)_3$. The trends of UV_{254} and DOC removal with pH were similar, showing a parabolic shape with the inflection point at 8, 7 and 7, for $TiCl_4$, $FeCl_3$ and $Al_2(SO_4)_3$, respectively. Both UV_{254} and DOC removal showed steady increase with pH at lower pH and then beyond the inflection point, the coagulation efficiency was either inhibited or even decreased with pH. The optimum initial solution pH for $TiCl_4$, $FeCl_3$ and $Al_2(SO_4)_3$ were 8, 7 and 7, respectively, under which condition the UV_{254} removal varied in the following order of $TiCl_4$ (54.9%) > $FeCl_3$ (47.6%) > $Al_2(SO_4)_3$ (41.2%) and the DOC removal followed the order of $FeCl_3$ (57.9%) > $TiCl_4$ (55.1%) > $Al_2(SO_4)_3$ (43.2%).

Fig. 2 also shows the variation of floc zeta potential at different solution pH for each coagulant. With the increasing pH value, the floc zeta potential decreased from positive to negative for both $TiCl_4$ and $FeCl_3$, while, for $Al_2(SO_4)_3$, it increased dramatically firstly from negative side to positive side and then nearly reached a plateau of around 4.0 mV. The difference in the effect of initial solution pH on floc zeta potential correlated well with the coagulant hydrolyzates. The relative importance of coagulation mechanisms for particle and organic matter removal depends primarily on pH. Generally, the main NOM removal mechanism at pH < 6 is dominated by complexation of NOM with soluble metal species into insoluble precipitates, while adsorption onto precipitated metal hydroxides dominated the mechanism at pH > 6 [36]. However, the possible dominant coagulation mechanisms varied with coagulant types and coagulation conditions.

For $TiCl_4$ and $FeCl_3$, at pH ⩽ 8, the negative charges of pollutants were possibly neutralized by the positively charged coagulant hydrolyzates, generating the flocs with positive charges due to excess of positively charged hydrolyzates adhering to the surface of aggregates. At pH > 8, bulk and rapid hydrolysis occurred, generating coagulation species with less positive charge, probably involving $Ti(OH)_4$ and $Fe(OH)_3$ precipitates. Thus, the $TiCl_4$ and $FeCl_3$ are unable to achieve complete neutralization, resulting in

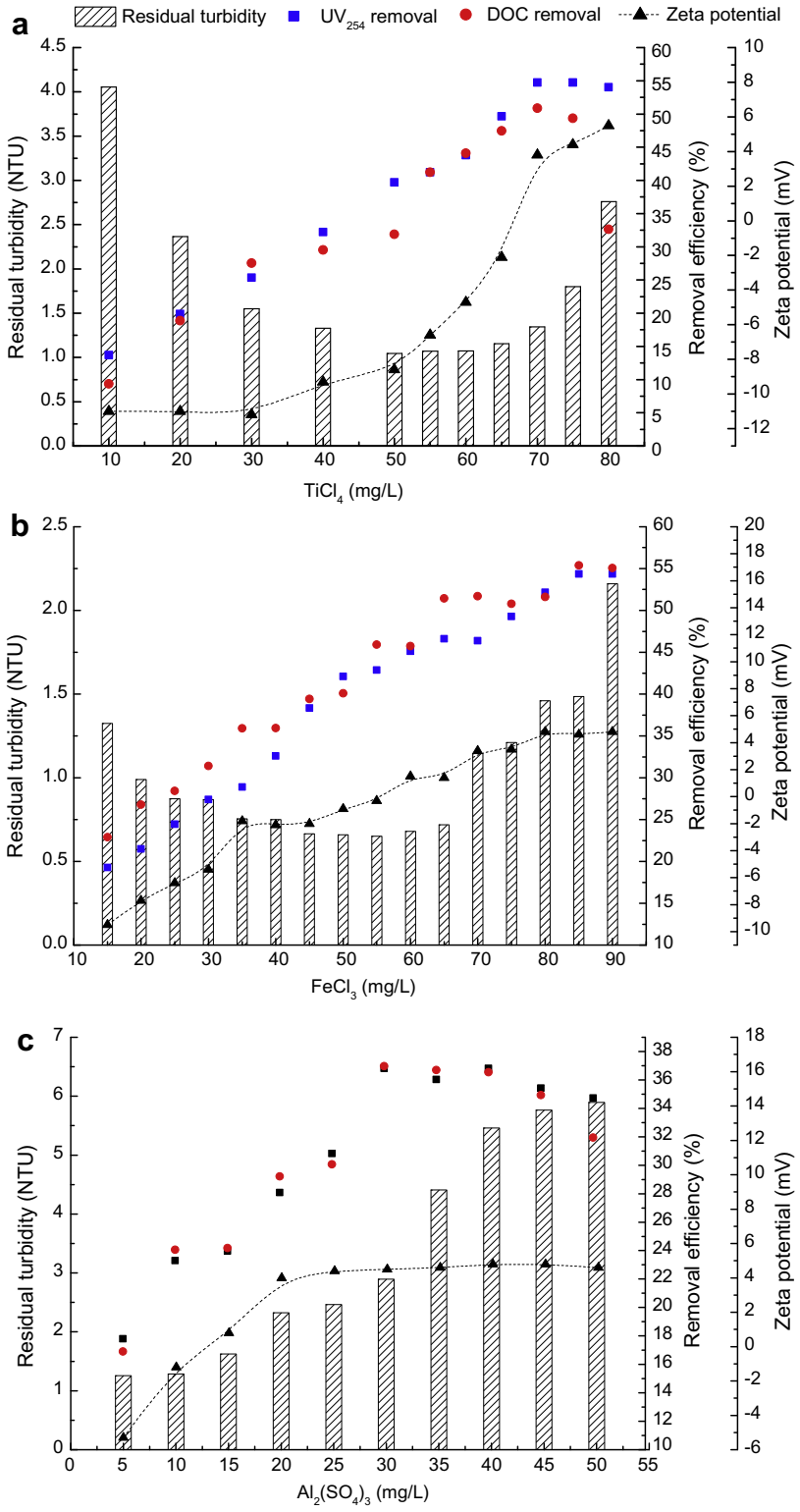

Fig. 1. Comparative coagulation/flocculation performances of the three coagulants: (a) $TiCl_4$; (b) $FeCl_3$ and (c) $Al_2(SO_4)_3$ all measured/assessed in terms of residual turbidity, UV_{254} removal, DOC removal and particle zeta potential.

the flocs with negative charges. This probably led to the decrease in UV_{254} and DOC removal at high pH values as shown in Fig. 2.

For $Al_2(SO_4)_3$, the polymerization was inhibited at pH < 5 and the positive monomer hydrolyzates dominated the Al speciation [37,38]. These positive hydrolyzates, such as $Al(OH)^{2+}$, $Al(OH)_2^+$, $Al_2(OH)_2^{4+}$, and $Al_3(OH)_4^{5+}$, easily neutralize the exterior negative charges of particles and organic matters, and further destabilized the colloids. However, the positive charges were not enough for full charge neutralization, yielding the flocs with negative charges. When the initial pH is between 6 and 9, the polymeric hydrolyzates with high positive charges and large surface area are formed [37,38]. The colloids are easily adsorbed, neutralized

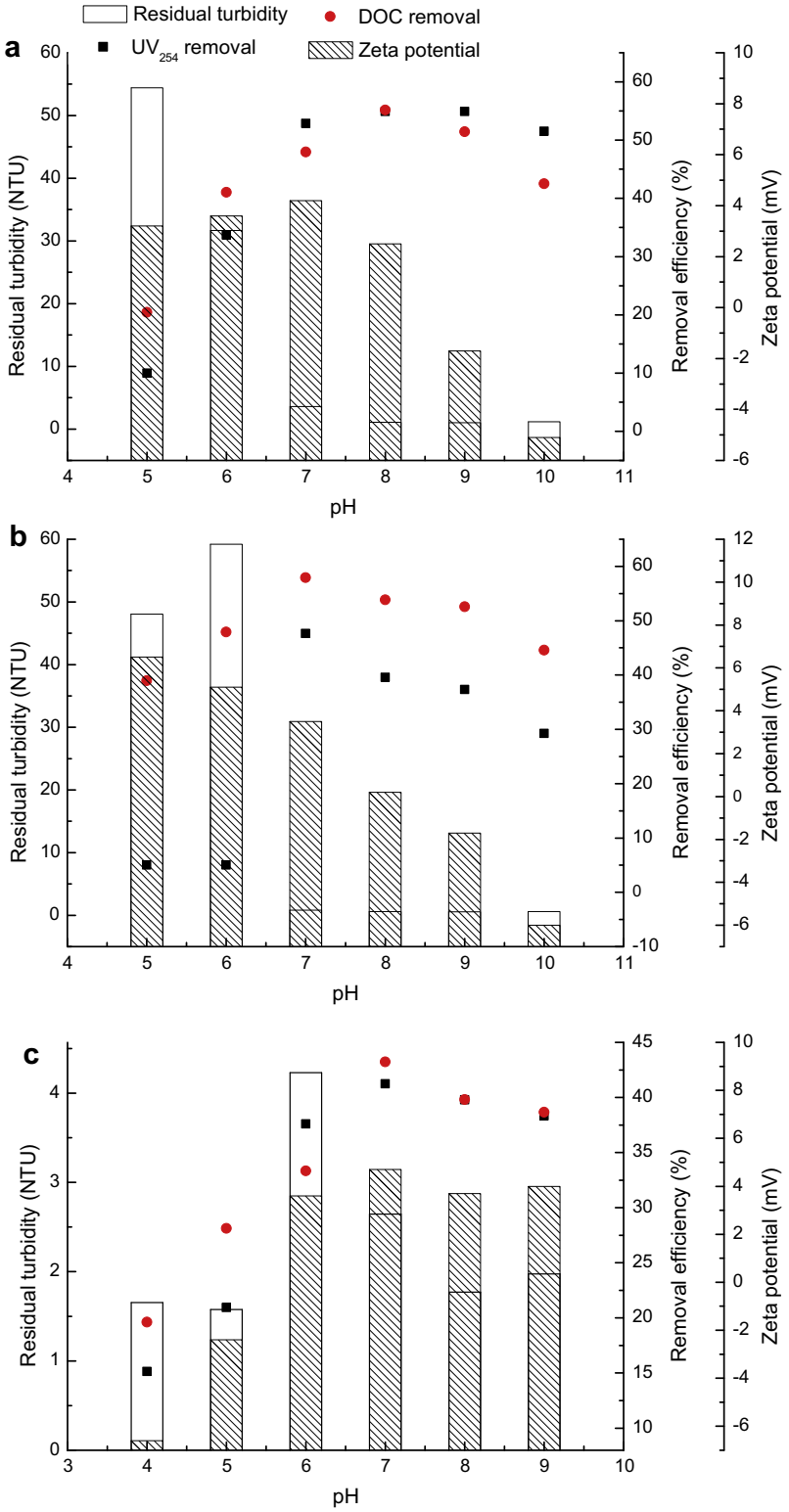

Fig. 2. The coagulation/flocculation performances of (a) $TiCl_4$; (b) $FeCl_3$ and (c) $Al_2(SO_4)_3$ under different initial pH and assessed in terms of residual turbidity, UV_{254} removal, DOC removal and particle zeta potential.

and co-precipitated by the hydrolyzates, producing the flocs with positive charges. For all the three coagulants, the slight decrease in UV_{254} and/or DOC removal at high pH values could be attributed to the mutual repulsion between particles with same charges.

3.3. Floc characterization

To understand the relative merits of different coagulants, the properties of the flocs formed by $TiCl_4$, $FeCl_3$ and $Al_2(SO_4)_3$ were investigated under optimum coagulant dose and solution pH

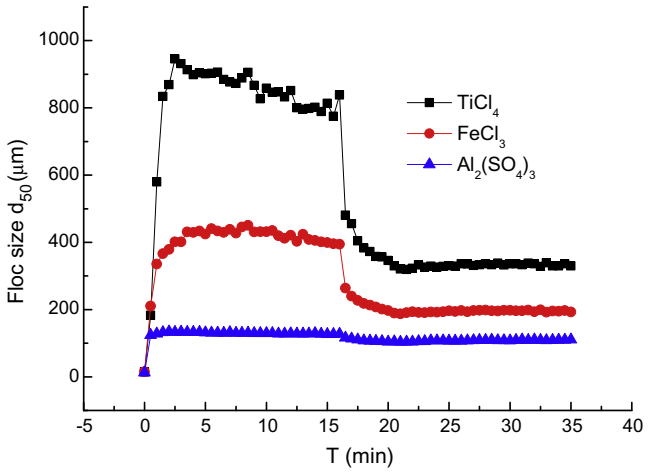

Fig. 3. Growth, breakage and regrowth of the flocs formed by different coagulants under optimum coagulant dose and initial pH conditions.

conditions. Fig. 3 presents the dynamic variation of floc size with time during coagulation process. The floc size quickly increased with time, reaching a steady stage during floc growth period, which was immediately reduced following an increase in shear. The flocs were broken to different degrees, and then began to regrow as the high shear was reduced again. The floc characteristics were then investigated in detail in terms of growth rate, size (d_1, d_2, and d_3), strength, recoverability and fractal dimension.

Table 1 summarizes the selected floc parameters under optimum coagulant dose and solution pH conditions. Compared to $FeCl_3$ and $Al_2(SO_4)_3$, $TiCl_4$ coagulant exhibited the highest floc growth rate at around 429.8 μm/min, which was approximately 3.5 times that by $FeCl_3$ and 6.5 times that by $Al_2(SO_4)_3$. The resultant flocs were with the largest size irrespective of the growth, breakage and regrowth process. Fig. 3 shows a sharp increase in size of the flocs by $TiCl_4$ coagulation during the first 2.5 min, achieving the largest floc size of around 950 μm. As the slow mixing continued, a slight decrease in floc size during the next 12.5 min was observed, which probably due to the disturbance of prolonged mixing on the aggregated flocs. Thus, the optimal duration of slow mixing is 2.5 min for $TiCl_4$ coagulation. The sharp increase in floc size was likely due to particles aggregation and the extended stirring may result in the breakage of the aggregated particles. In contrast, the flocs formed by $FeCl_3$ and $Al_2(SO_4)_3$ were more stable and floc breakage seldom appeared during slow stir mixing phase.

Floc strength factor (S_f) and recovery factor (R_f), calculated by Eqs. (2) and (3), were used to evaluate the floc strength and recoverability. Both S_f and R_f of flocs formed by the three coagulants varied apparently in the following order of $Al_2(SO_4)_3$ > $FeCl_3$ > $TiCl_4$ (Table 1). Based on Jarvis et al. [27], the larger flocs are more prone to be affected by microscale eddies which resulted in floc breakage, while the smaller ones were more likely to be entrained within eddies rather than be broken by them. That probably led to the decrease of floc strength for $TiCl_4$ since it has the largest floc sizes initially. On the contrary, flocs formed by $Al_2(SO_4)_3$ were with the smallest size but the best ability to stand shear as reflected by the highest S_f value, which agreed well with the general conception that the smaller flocs tend to show greater floc strength than the larger ones [39]. As mentioned earlier, the polymeric Al hydrolyzates may have been formed under the optimum condition and the polymerized Al_{13} aggregates may be another reason that enhanced the floc strength [40]. Additionally, the flocs formed by charge neutralization are expected to give full recovery after floc breakage, while the sweep flocs showed poor regrowth [10,41]. The R_f values for the three coagulants were all lower than 100%, indicating that the sweep flocculation was an important coagulation mechanism involved besides charge neutralization for these coagulants. This is in accordance with the conclusions drawn earlier in Sections 3.1 and 3.2. In comparison to the conventional $FeCl_3$ and $Al_2(SO_4)_3$ coagulants, the $TiCl_4$ flocs showed the worst regrowth after breakage as demonstrated by the lowest R_f value.

Moreover, the floc fractal dimension was investigated to compare the floc compaction degree with different coagulants. Analysis of floc fractal structure with the three coagulants showed the floc D_f values followed the order of $TiCl_4 \approx FeCl_3 > Al_2(SO_4)_3$. Generally, the larger the floc size, the smaller the fractal dimension [26]. However, irrespective of floc growth, breakage or regrowth process, $TiCl_4$ and $FeCl_3$ yielded the flocs with higher D_f values than $Al_2(SO_4)_3$, although the flocs formed by $TiCl_4$ and $FeCl_3$ were larger than those by $Al_2(SO_4)_3$. Based on the results obtained, the $TiCl_4$ flocs are with higher growth rate, larger size and higher floc compaction degree, which is of great significance on sedimentation, flotation and filtration process after the coagulation/flocculation process [8].

3.4. Membrane fouling in coagulation–ultrafiltration (C–UF) hybrid process

The effluent after $TiCl_4$, $FeCl_3$ and $Al_2(SO_4)_3$ coagulation under optimum dose and solution pH conditions were used as the feed water for ultrafiltration to evaluate the membrane fouling potentials of the treated water. Fig. 4 presents the normalized fluxes associated with filtration time. The fluxes first shows dramatic decrease with time in all cases, and then the decline at a reduced scale was observed. A significant difference of flux variation can be seen when the suspension was pre-coagulated with different coagulants. The three coagulants resulted in distinct membrane permeate fluxes and the severity of flux decline followed the order of $Al_2(SO_4)_3$ < $FeCl_3$ < $TiCl_4$.

The floc properties have been proved to markedly influence the membrane fouling [22,23,42]. Since particle size is inversely proportional to cake resistance [42], the resultant flux decline for $Al_2(SO_4)_3$ was supposed to be the severest among the three coagulants due to the smallest floc size (Table 1). However, this did not agree with the results shown in Fig. 4. As stated by Wang et al. [43], the flocs with lower D_f values produce less resistance and thus are beneficial for membrane permeability, while the compact ones with larger D_f lead to high level of resistance during ultrafiltration. Compared to $FeCl_3$ and $TiCl_4$, the $Al_2(SO_4)_3$ coagulant produced the flocs with the lowest degree of compaction given the lowest D_f value

Table 1
Selected floc parameters under optimum coagulant dose and pH conditions.

Coagulant	Floc growth rate (μm/min)	d_1 (μm)	d_2 (μm)	d_3 (μm)	S_f (%)	R_f (%)	D_f		
							Before breakage	After breakage	After regrowth
$TiCl_4$	429.8	859.7	320.6	334.0	37.3	2.5	2.44	2.52	2.52
$FeCl_3$	120.8	422.9	187.5	196.3	44.3	3.8	2.49	2.55	2.56
$Al_2(SO_4)_3$	65.1	130.2	103.9	108.3	79.8	16.6	2.23	2.25	2.25

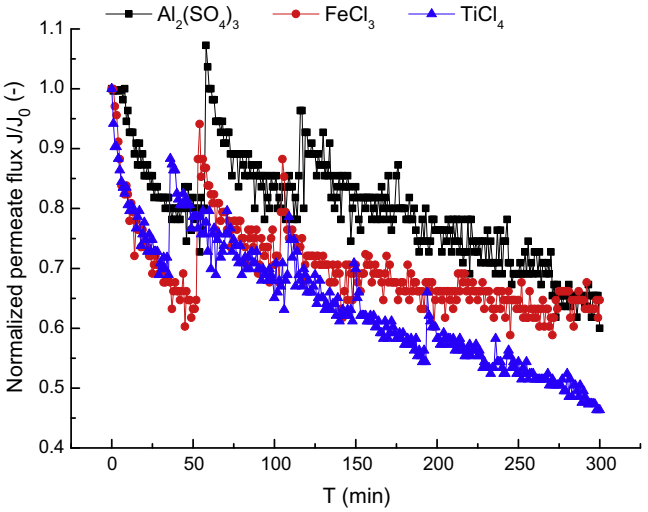

Fig. 4. Normalized ultrafiltration permeate flux profiles with different coagulants under optimum dose conditions.

(Table 1). Therefore, the loosely structured aggregates formed by $Al_2(SO_4)_3$ were actually helping reduce membrane fouling. The most severe flux decline occurred with $TiCl_4$ as pre-coagulant, which could be ascribed to the weakest floc strength. The flocs with weak strength are more likely to be destroyed by the turbulence flow and/or microscale eddies in the coagulation system and leave more aggregates fractions in the feed water. The desquamated fragments would promote the formation of cake layer, which subsequently would aggravate the flux decline [18]. The highest strength of the $Al_2(SO_4)_3$ flocs was another reason for the lower decline of normalized flux. The severity of permeate flux seems consistent with the sequence of floc strength on the whole [18].

3.5. Characterization of the flocculated sludge

3.5.1. Crystal structure analysis (XRD)

To recycle the $TiCl_4$ flocculated sludge, the settled flocs produced after $TiCl_4$ coagulation was incinerated at different temperatures between 200 °C and 1000 °C. The incinerated sludge changed from black to white with the increase in temperature. The black color might be attributed to the remaining organic matter at low temperatures.

XRD images were analyzed to identify the crystal structure of particles after incineration. The XRD image of the commercially available TiO_2 (P-25) was also investigated for comparison. As shown in Fig. 5a, apparent anatase structure can be observed at 600 °C, and at 800 °C while at 1000 °C, the rutile phase appeared. The amorphous structure observed below 600 °C may be due to the remaining organic matter. P-25 showed the mixture of both anatase and rutile TiO_2. The TiO_2 with anatase structure is generally accepted as the most active and efficient photocatalyst compared to rutile and brookite [44]. Therefore, the TiO_2 obtained at 600 °C is expected to be an efficient photocatalyst, which coincides with Lee et al. [4] and Okour et al. [45]. Here, the 600 °C was selected as the most efficient temperature taking into account the energy require to recover the photocatalyst from the sludge.

3.5.2. Thermal analysis (TG/DSC)

The thermogram recorded for the settled flocs after $TiCl_4$ coagulation is shown in Fig. 5b. A continuous weight loss distributed between 25 and 557.39 °C in the TG plot can be seen. The thermal treatment of sludge up to 153.77 °C led mainly to the loss of adsorbed water content (16.65%) while it resulted in the removal

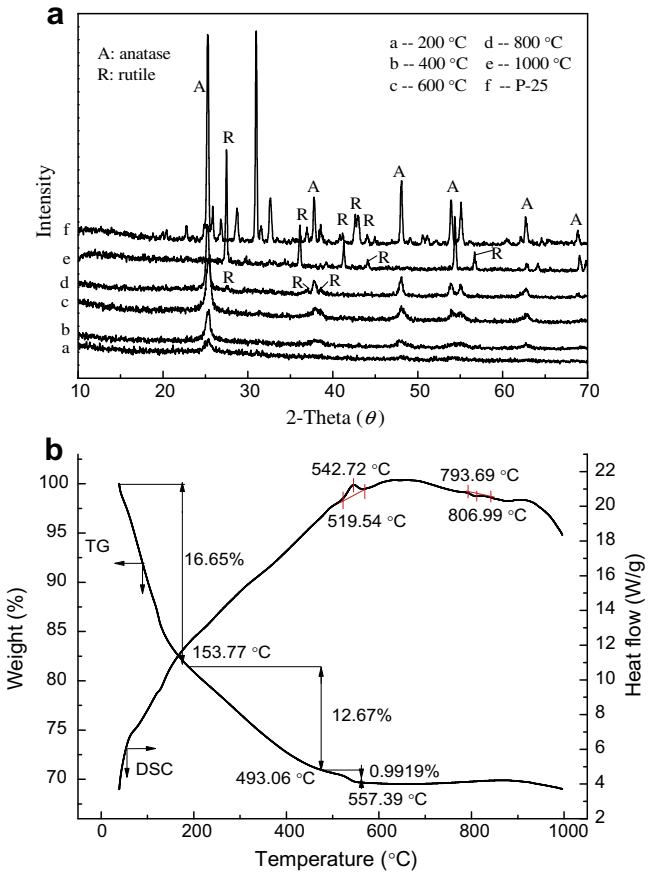

Fig. 5. The settled $TiCl_4$ flocs: (a) XRD image of particles after incineration under different temperatures conditions; (b) thermal analysis (TG: thermogravimetry; DSC: different scanning calorimetry).

of organic matter (12.67%) between 153.77 and 493.06 °C. Another weight loss of 0.9919% at 493.06–557.39 °C may be caused by the release of constitution water.

The DSC curve of the settled flocs was comparatively smooth and there were no obvious peaks except at 542.72 °C and 806.99 °C. The transformed temperature of the anatase phase to rutile was approximately 550 °C according to Liao et al. [46]. However, this transformation occurred at approximately 800 °C according to results of XRD analysis (Fig. 5a), corresponding well with the endothermic peak at 806.99 °C. The peak at 542.72 °C was speculated to be the indication of transformation from amorphous structure to apparent anatase phase of TiO_2. This is in agreement with the obvious anatase TiO_2 at 600 °C shown in Fig. 5a.

3.5.3. SEM analysis

As mentioned in Section 3.5.1, the 600 °C was selected as the optimum temperature for incineration and the TiO_2 produced at this temperature is referred to as "as-prepared TiO_2". The SEM photographs of as-prepared TiO_2 and P-25 TiO_2 with different magnifications are shown in Fig. 6. The P-25 TiO_2 was nearly spherically shaped and almost has uniform size distribution (Fig. 6d and e). However, for as-prepared TiO_2, irregular structure was observed (Fig. 6a), which may be due to the large amount of impurities (in terms of organic compounds) found in Xiaoqing River. From SEM images with 3.00 K of magnification (Fig. 6b and c), the impurities attaching on the surface of the as-prepared TiO_2 resulted in the rough appearance. The impurity ratio of TiO_2 nanoparticles (doped with carbon and phosphorus) from wastewater, was approximately 20% as Shon et al. reported [3].

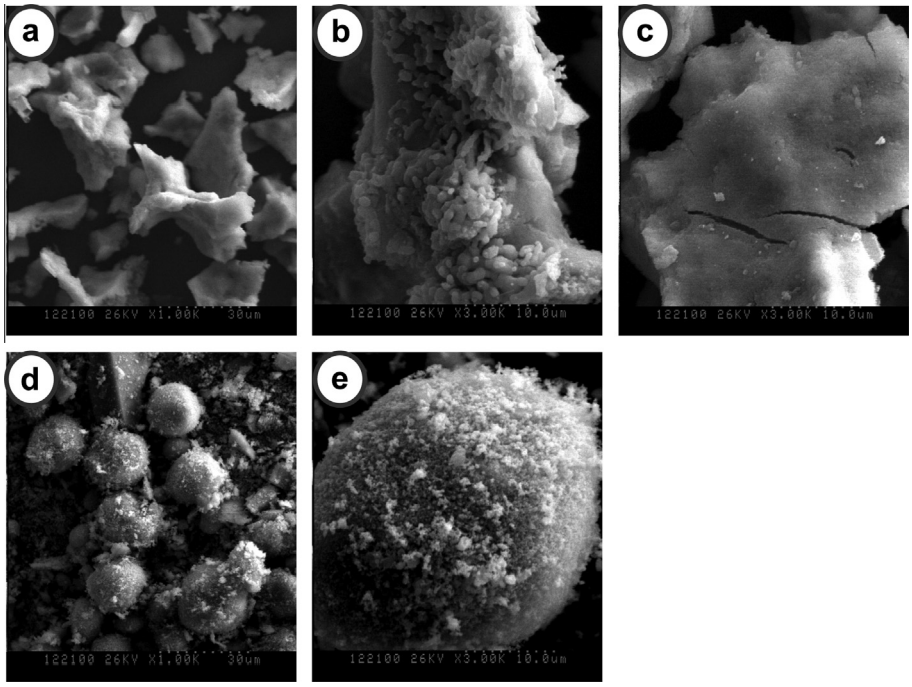

Fig. 6. SEM images of as-prepared TiO_2 and P-25 TiO_2 with different magnifications: (a) as-prepared TiO_2, 1.00 K; (b and c) as-prepared TiO_2, 3.00 K; (d) P-25 TiO_2, 1.00 K; (e) P-25 TiO_2, 3.00 K.

4. Conclusions

Coagulation behavior, floc properties and membrane fouling potential for the three different coagulants ($TiCl_4$, $FeCl_3$, and $Al_2(SO_4)_3$) were studied for the real water treatment. The $TiCl_4$ coagulated sludge was collected and then recycled to produce TiO_2, which was subsequently characterized by XRD, TG/DSC and SEM. The following conclusions can be drawn:

1. $TiCl_4$ was an effective coagulant for real water treatment, with the UV_{254} removal varied in the following order of $TiCl_4$ (54.9%) > $FeCl_3$ (47.6%) > $Al_2(SO_4)_3$ (41.2%) and the DOC removal followed the order of $FeCl_3$ (57.9%) > $TiCl_4$ (55.1%) > $Al_2(SO_4)_3$ (43.2%).
2. The $TiCl_4$ flocs exhibited higher growth rate and larger the floc size than those by $FeCl_3$, and $Al_2(SO_4)_3$. However, the $TiCl_4$ flocs showed the lowest S_f and R_f values, indicating the weakest ability to withstand shear and the worst re-growth after breakage.
3. Analysis of floc fractal structure with the three coagulants showed the floc D_f values followed the order of $TiCl_4 \approx FeCl_3 > Al_2(SO_4)_3$, indicating the higher compactness of flocs formed by $TiCl_4$ and $FeCl_3$.
4. The investigation of membrane fouling demonstrated that $Al_2(SO_4)_3$ precoagulation resulted in least membrane fouling potential, while the most severe flux decline was observed for the effluent after $TiCl_4$ coagulation.
5. The $TiCl_4$ coagulated sludge can be recycled to produce anatase TiO_2. According to SEM results, the as-prepared TiO_2 was with irregular surface structure, while the P-25 TiO_2 was nearly spherically shaped.

Acknowledgements

This work was supported by a grant from the Chinese National Natural Science Foundation (No. 51278283), Australia Research Council Discovery Projects (ARC DP), the Shanghai Tongji Gao Tingyao Environmental Science & Technology Development Foundation (STGEF) and the scholarship from China Scholarship Council.

Appendix A. Supplementary material

Supplementary data associated with this article can be found, in the online version, at http://dx.doi.org/10.1016/j.seppur.2014.04.015.

References

[1] C. Hu, H. Liu, J. Qu, D. Wang, J. Ru, Coagulation behavior of aluminum salts in eutrophic water: significance of Al_{13} species and pH control, Environ. Sci. Technol. 40 (2006) 325–331.
[2] H. Shon, S. Vigneswaran, J. Kandasamy, M. Zareie, J. Kim, D. Cho, J.H. Kim, Preparation and characterization of titanium dioxide (TiO_2) from sludge produced by $TiCl_4$ flocculation with $FeCl_3$, $Al_2(SO_4)_3$ and $Ca(OH)_2$ coagulant aids in wastewater, Sep. Sci. Technol. 44 (2009) 1525–1543.
[3] H. Shon, S. Vigneswaran, I.S. Kim, J. Cho, G. Kim, J. Kim, J.H. Kim, Preparation of titanium dioxide (TiO_2) from sludge produced by titanium tetrachloride ($TiCl_4$) flocculation of wastewater, Environ. Sci. Technol. 41 (2007) 1372–1377.
[4] B. Lee, S. Kim, H. Shon, S. Vigneswaran, S. Kim, J. Cho, I.S. Kim, K. Choi, J. Kim, H. Park, Aquatic toxicity evaluation of TiO_2 nanoparticle produced from sludge of $TiCl_4$ flocculation of wastewater and seawater, J. Nanopart. Res. 11 (2009) 2087–2096.
[5] M.R. Hoffmann, S.T. Martin, W. Choi, D.W. Bahnemann, Environmental applications of semiconductor photocatalysis, Chem. Rev. 95 (1995) 69–96.
[6] T.N. Obee, R.T. Brown, TiO_2 photocatalysis for indoor air applications: effects of humidity and trace contaminant levels on the oxidation rates of formaldehyde, toluene, and 1,3-butadiene, Environ. Sci. Technol. 29 (1995) 1223–1231.
[7] WHO, Environmental Health Criteria (24), 1982. <http://toxnet.nlm-.nih.gov/cgi-bin/sis/search/f?./temp/THVY88:1> (The easiest access to this source is by the Internet).
[8] W. Yu, G. Li, Y. Xu, X. Yang, Breakage and re-growth of flocs formed by alum and PACl, Powder Technol. 189 (2009) 439–443.
[9] P. Jarvis, B. Jefferson, S.A. Parsons, How the natural organic matter to coagulant ratio impacts on floc structural properties, Environ. Sci. Technol. 39 (2005) 8919–8924.
[10] M. Aguilar, J. Saez, M. Llorens, A. Soler, J. Ortuno, Microscopic observation of particle reduction in slaughterhouse wastewater by coagulation–flocculation using ferric sulphate as coagulant and different coagulant aids, Water Res. 37 (2003) 2233–2241.
[11] C.P. Johnson, X. Li, B.E. Logan, Settling velocities of fractal aggregates, Environ. Sci. Technol. 30 (1996) 1911–1918.

[12] X. Li, B.E. Logan, Collision frequencies between fractal aggregates and small particles in a turbulently sheared fluid, Environ. Sci. Technol. 31 (1997) 1237–1242.
[13] C. Jucker, M.M. Clark, Adsorption of aquatic humic substances on hydrophobic ultrafiltration membranes, J. Membr. Sci. 97 (1994) 37–52.
[14] A. Zularisam, A. Ismail, R. Salim, Behaviours of natural organic matter in membrane filtration for surface water treatment – a review, Desalination 194 (2006) 211–231.
[15] C. Guigui, J. Rouch, L. Durand-Bourlier, V. Bonnelye, P. Aptel, Impact of coagulation conditions on the in-line coagulation/UF process for drinking water production, Desalination 147 (2002) 95–100.
[16] P.-K. Park, C.-H. Lee, S.-J. Choi, K.-H. Choo, S.-H. Kim, C.-H. Yoon, Effect of the removal of DOMs on the performance of a coagulation–UF membrane system for drinking water production, Desalination 145 (2002) 237–245.
[17] J.-I. Oh, Influence of streaming potential on flux decline of microfiltration with in-line rapid pre-coagulation process for drinking water production, J. Membr. Sci. 254 (2005) 39–47.
[18] W. Xu, B. Gao, R. Mao, Q. Yue, Influence of floc size and structure on membrane fouling in coagulation–ultrafiltration hybrid process – the role of Al_{13} species, J. Hazard. Mater. 193 (2011) 249–256.
[19] W. Xu, B. Gao, Effect of shear conditions on floc properties and membrane fouling in coagulation/ultrafiltration hybrid process – the significance of Al_b species, J. Membr. Sci. 415–416 (2012) 153–160.
[20] A. Pikkarainen, S. Judd, J. Jokela, L. Gillberg, Pre-coagulation for microfiltration of an upland surface water, Water Res. 38 (2004) 455–465.
[21] A. Schäfer, A.G. Fane, T. Waite, Fouling effects on rejection in the membrane filtration of natural waters, Desalination 131 (2000) 215–224.
[22] T.D. Waite, A.I. Schäfer, A.G. Fane, A. Heuer, Colloidal fouling of ultrafiltration membranes: impact of aggregate structure and size, J. Colloid Interface Sci. 212 (1999) 264–274.
[23] K.Y. Choi, B.A. Dempsey, In-line coagulation with low-pressure membrane filtration, Water Res. 38 (2004) 4271–4281.
[24] Y. Zhao, B. Gao, H. Shon, B. Cao, J.H. Kim, Coagulation characteristics of titanium (Ti) salt coagulant compared with aluminum (Al) and iron (Fe) salts, J. Hazard. Mater. 185 (2011) 1536–1542.
[25] F. Xiao, P. Yi, X.R. Pan, B.J. Zhang, C. Lee, Comparative study of the effects of experimental variables on growth rates of aluminum and iron hydroxide flocs during coagulation and their structural characteristics, Desalination 250 (2010) 902–907.
[26] B. Cao, B. Gao, X. Liu, M. Wang, Z. Yang, Q. Yue, The impact of pH on floc structure characteristic of polyferric chloride in a low DOC and high alkalinity surface water treatment, Water Res. 45 (2011) 6181–6188.
[27] P. Jarvis, B. Jefferson, S.A. Parsons, Breakage, regrowth, and fractal nature of natural organic matter flocs, Environ. Sci. Technol. 39 (2005) 2307–2314.
[28] Y. Zhao, B. Gao, H. Shon, Y. Wang, J.H. Kim, Q. Yue, X. Bo, Anionic polymer compound bioflocculant as a coagulant aid with aluminum sulfate and titanium tetrachloride, Bioresour. Technol. 108 (2012) 45–54.
[29] J.L. Lin, C. Huang, C.J.M. Chin, J.R. Pan, Coagulation dynamics of fractal flocs induced by enmeshment and electrostatic patch mechanisms, Water Res. 42 (2008) 4457–4466.
[30] J. Wei, B. Gao, Q. Yue, Y. Wang, W. Li, X. Zhu, Comparison of coagulation behavior and floc structure characteristic of different polyferric-cationic polymer dual-coagulants in humic acid solution, Water Res. 43 (2009) 724–732.
[31] T.P. Rieker, M. Hindermann-Bischoff, F. Ehrburger-Dolle, Small-angle X-ray scattering study of the morphology of carbon black mass fractal aggregates in polymeric composites, Langmuir 16 (2000) 5588–5592.
[32] C. Ye, D. Wang, B. Shi, J. Yu, J. Qu, M. Edwards, H. Tang, Alkalinity effect of coagulation with polyaluminum chlorides: role of electrostatic patch, Colloid Surf. A – Physicochem. Eng. Asp. 294 (2007) 163–173.
[33] I. Licsko, On the types of bond developing between the aluminium and iron (III) hydroxides and organic substances, Water Sci. Technol. 27 (1993) 249–252.
[34] W. Mekhamer, F. Assaad, Flocculation and coagulation of Ca-and K-saturated montmorillonite in the presence of polyethylene oxide, J. Appl. Polym. Sci. 73 (1999) 659–662.
[35] J. Gregory, J. Duan, Hydrolyzing metal salts as coagulants, Pure Appl. Chem. 73 (2001) 2017–2026.
[36] J. Gregor, C. Nokes, E. Fenton, Optimising natural organic matter removal from low turbidity waters by controlled pH adjustment of aluminium coagulation, Water Res. 31 (1997) 2949–2958.
[37] P. Zhang, Z. Wu, G. Zhang, G. Zeng, H. Zhang, J. Li, X. Song, J. Dong, Coagulation characteristics of polyaluminum chlorides PAC-Al_{30} on humic acid removal from water, Sep. Purif. Technol. 63 (2008) 642–647.
[38] B. Corain, G. Bombi, A. Tapparo, M. Perazzolo, P. Zatta, Aluminium toxicity and metal speciation: established data and open questions, Coordin. Chem. Rev. 149 (1996) 11–22.
[39] P. Jarvis, B. Jefferson, J. Gregory, S.A. Parsons, A review of floc strength and breakage, Water Res. 39 (2005) 3121–3137.
[40] X. Wu, D. Wang, X. Ge, H. Tang, Coagulation of silica microspheres with hydrolyzed Al (III) – significance of Al_{13} and Al_{13} aggregates, Colloid Surf. A – Physicochem. Eng. Asp. 330 (2008) 72–79.
[41] V. Chaignon, B. Lartiges, A. El Samrani, C. Mustin, Evolution of size distribution and transfer of mineral particles between flocs in activated sludges: an insight into floc exchange dynamics, Water Res. 36 (2002) 676–684.
[42] K. Listiarini, D.D. Sun, J.O. Leckie, Organic fouling of nanofiltration membranes: evaluating the effects of humic acid, calcium, alum coagulant and their combinations on the specific cake resistance, J. Membr. Sci. 332 (2009) 56–62.
[43] J. Wang, J. Guan, S. Santiwong, T.D. Waite, Characterization of floc size and structure under different monomer and polymer coagulants on microfiltration membrane fouling, J. Membr. Sci. 321 (2008) 132–138.
[44] A. Fujishima, T.N. Rao, D.A. Tryk, Titanium dioxide photocatalysis, J. Photochem. Photobiol. C: Photochem. Rev. 1 (2000) 1–21.
[45] Y. Okour, I. El Saliby, H. Shon, S. Vigneswaran, J.-H. Kim, J. Cho, I.S. Kim, Recovery of sludge produced from Ti-salt flocculation as pretreatment to seawater reverse osmosis, Desalination 247 (2009) 53–63.
[46] S. Liao, W. Mayo, K. Pae, Theory of high pressure/low temperature sintering of bulk nanocrystalline TiO_2, Acta Mater. 45 (1997) 4027–4040.